Available on CMS information server

CMS NOTE 2006/023

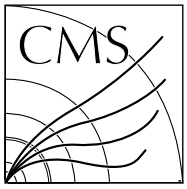

The Compact Muon Solenoid Experiment

CMS Note

Mailing address: CMS CERN, CH-1211 GENEVA 23, Switzerland

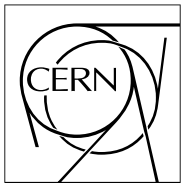

30th of January 2006

Fitting of Event Topologies with External Kinematic Constraints in CMS

J. D'Hondt, S. Lowette

Vrije Universiteit Brussel (VUB-IIHE), Brussels, Belgium

O. Buchmüller, S. Cucciarelli, F.-P. Schilling, M. Spiropulu

CERN, Geneva, Switzerland

S. Paktinat Mehdiabadi

Sharif University of Technology & IPM, Tehran, Iran

D. Benedetti

Università di Perugia and INFN, Perugia, Italy

L. Pape

Institut fur Teilchenphysik, Eidgenossische Technische Hochschule (ETH), Zurich, Switzerland

Abstract

The resolution of the measured objects in the final state of proton collisions at the Large Hadron Collider can be improved by forcing well-defined kinematic hypotheses on the event. The kinematic constraints proposed by the hypotheses can be applied by means of Lagrange multipliers in a general event-by-event least square fitting technique. The resulting chi-square of the fit can be interpreted as the probability of the proposed kinematic hypotheses to be true for the observed event. This note describes both the general mathematical concept of kinematic fitting and its implementation within the analysis framework of the Compact Muon Solenoid experiment. The performance of the method is demonstrated in a few typical case-studies where relative improvements are emphasized.

1 Introduction

The application of constraint kinematic fitting methods in particles physics has a very long history. In particular at LEP-2 and the B-factories this analysis technique became a frequently used tool for the reconstruction of entire or partial event topologies. Due to the accurate measurement of the incoming electron and positron momenta at e^+e^- colliders, applying constraints of energy and momentum conservation has usually led to significantly improved estimators of the kinematics of the underlying event processes.

The reconstruction of the mass of the W boson at LEP-2 in the event topologies $e^+e^- \to W^+W^- \to q\bar{q}Q\bar{Q}$ and $e^+e^- \to W^+W^- \to q\bar{q}l\nu_l$ improved significantly due to the application of energy and momentum constraints between initial and final states [1].

Another example of a full kinematic reconstruction on an entire event topology is semileptonic B decays at the Y_{4s} experiments [2, 3, 4]. In BaBar, the kinematic fit package presented here is used to improve the reconstruction of $B\bar{B} \to D^{(*)}n\pi\, X_{c/u}l\nu$ decays where one B hadron decays hadronically and the other B leptonically. The use of the kinematic fit for this semileptonic decay topology has resulted in a significant improvement of the invariant mass resolution of the $X_{c/u}$ and, therefore, greatly improved the measurements of the CKM matrix elements V_{cb} and V_{ub}.

Kinematic fitting techniques have also been applied to verify a hypothetical kinematic topology, as for example in the search for the Standard Model Higgs boson at LEP-2 [5].

Although at proton colliders, like the LHC, these powerful constraints between initial and final state kinematics are not available, the use of constraint kinematic fitting tools is still possible for various cases. In this note we will demonstrate in a few examples of CMS analyses that the application of well-defined kinematic constraints can lead to significant improvements.

The next Section will overview the mathematics of the general non-linear least square fit technique using Lagrange multipliers. In Section 3 the Monte Carlo simulations used for obtaining the results in this paper are described. The improvement on several reconstructed variables is illustrated from Section 4 until Section 7. These Sections show in several physics cases and by the use of different parametrizations of the 4-vectors of jets and leptons, the usefulness of applying kinematic fits in improving the result. A summary including recommendations is mentioned in Section 8.

2 The General Non-Linear Least Square Fit Concept using Lagrange Multipliers

A physical problem in many cases consists of measured quantities as particles' four-vectors and unmeasured values. While the measured quantities typically represent 4-vector estimators of certain reconstructed objects (e.g jets, tracks, etc), the unmeasured quantities are supposed to mark the undetected particles of the underlying primary event structure (e.g. neutrinos). Also one often has a certain hypothesis for an event. Then constraints like energy and momentum conservation can be used to slightly change the measured values within the uncertainties to fulfil these kinematic requirements. This procedure one usually calls a *kinematic fit*, which is applied by a least square method.

Below the basic framework for kinematic fitting is sketched, while a more comprehensive and detailed description can be found in [6]. Subsection 2.1 gives a general overview about the notation and the solution of the given task. The constraints $\vec{f}$ sometimes depend in a non-linear way on the parameters which are fitted. In this case the χ^2-minimization can only be solved iteratively. This procedure is described in subsection 2.2.

2.1 Introduction

Let us assume we have to solve a problem with n measured parameters $\vec{y}$, p unmeasured parameters $\vec{a}$ and m constraints $\vec{f}$ as defined in eq. 1. These requirements will be fulfilled for the true parameters $\bar{a}$ and $\bar{y}$.

$$\begin{aligned} f_1(\bar{a}_1,\bar{a}_2,\ldots,\bar{a}_p,\bar{y}_1,\bar{y}_2,\ldots,\bar{y}_n) &= 0 \\ f_2(\bar{a}_1,\bar{a}_2,\ldots,\bar{a}_p,\bar{y}_1,\bar{y}_2,\ldots,\bar{y}_n) &= 0 \\ &\vdots \\ f_m(\bar{a}_1,\bar{a}_2,\ldots,\bar{a}_p,\bar{y}_1,\bar{y}_2,\ldots,\bar{y}_n) &= 0 \end{aligned} \tag{1}$$

In general the measured values $\vec{y}$ will not fulfil the constraints, so that one has to calculate corrections $\Delta\vec{y}$. Then the sum $\vec{y}' = \vec{y} + \Delta\vec{y}$ will fulfill the constraints. In the same step, the weighted sum

$$S(\vec{y}) = \Delta\vec{y}^T \mathcal{V}^{-1} \Delta\vec{y} \tag{2}$$

should be minimal with $\mathcal{V}$ being the covariance matrix of the measured parameters.

A general method to determine local extrema of non-linear functions of many variables is by using the definition of *Langrange Multipliers*. The likelihood of this new problem is defined as follows:

$$L(\vec{y}, \vec{a}, \vec{\lambda}) = S(\vec{y}) + 2 \sum_{k=1}^{m} \lambda_k f_k(\vec{y}, \vec{a}) \tag{3}$$

with $\vec{\lambda}$ the Lagrange Multipliers. The necessary condition for a local minimum of this function is then equivalent to the condition for a minimum of $S(\vec{y})$ under the constraint $f_k(\vec{y}, \vec{a}) = 0$.

With linear constraints the solution can be found in one step, otherwise it has to be found iteratively. This means that in every iteration the problem is linearized as described in subsection 2.2.

2.2 Linearization

In this subsection the linearization and solution of eq. 3 will be described. The linearized constraints are given in eq. 4 in which the following notation is used:

$\vec{y}/\vec{a}$	$\rightarrow$	start values of measured/ unmeasured parameters
$\vec{y}^*/\vec{a}^*$	$\rightarrow$	values of the measured/ unmeasured parameters after the last iteration
$\vec{y}'/\vec{a}'$	$\rightarrow$	values of the measured/ unmeasured parameters after the current iteration
$\Delta\vec{y}^*/\Delta\vec{a}^*$	$\rightarrow$	$\vec{y}^* - \vec{y}$ resp. $\vec{a}^* - \vec{a}$
$\Delta\vec{y}/\Delta\vec{a}$	$\rightarrow$	$\vec{y}' - \vec{y}$ resp. $\vec{a}' - \vec{a}$

$$\begin{aligned} f_k(\vec{y}', \vec{a}') \approx f(\vec{y}^*, \vec{a}^*) \quad &+ \quad \sum_{j=1}^{p} \frac{\partial f_k}{\partial a_j} \cdot (\Delta a_j - \Delta a_j^*) \\ &+ \quad \sum_{i=1}^{n} \frac{\partial f_k}{\partial y_i} \cdot (\Delta y_i - \Delta y_i^*) \approx 0 \quad . \end{aligned} \tag{4}$$

The derivatives are calculated at $(\vec{y}^*, \vec{a}^*)$. These equations can be written in vector notation,

$$\vec{f}^* + \mathcal{A}(\Delta\vec{a} - \Delta\vec{a}^*) + \mathcal{B}(\Delta\vec{y} - \Delta\vec{y}^*) \approx 0, \tag{5}$$

or

$$\mathcal{A}\Delta\vec{a} + \mathcal{B}\Delta\vec{y} - \vec{c} = 0 \qquad \text{with} \qquad \vec{c} = \mathcal{A}\Delta\vec{a}^* + \mathcal{B}\Delta\vec{y}^* - \vec{f}^*. \tag{6}$$

The vector $\vec{c}$ in eq. 6 is for iteration n a constant vector which only depends on quantities of the previous iteration $(n-1)$. In equation 5 and 6 the matrices $\mathcal{A}$ and $\mathcal{B}$ are defined as follows:

$$\mathcal{A} = \frac{\partial \vec{f}}{\partial \vec{a}} \qquad \mathcal{B} = \frac{\partial \vec{f}}{\partial \vec{y}} \quad . \tag{7}$$

So one big part of the work is to calculate the derivatives of the constraints with respect to the parameters $\vec{a}$ and $\vec{y}$. For illustration we give the components of the matrices:

$$\mathcal{A} = \begin{pmatrix} \partial f_1/\partial a_1 & \partial f_1/\partial a_2 & \dots & \partial f_1/\partial a_p \\ \partial f_2/\partial a_1 & \partial f_2/\partial a_2 & \dots & \partial f_2/\partial a_p \\ \vdots & & & \\ \partial f_m/\partial a_1 & \partial f_m/\partial a_2 & \dots & \partial f_m/\partial a_p \end{pmatrix} \tag{8}$$

$$\mathcal{B} = \begin{pmatrix} \partial f_1/\partial y_1 & \partial f_1/\partial y_2 & \dots & \partial f_1/\partial y_n \\ \partial f_2/\partial y_1 & \partial f_2/\partial y_2 & \dots & \partial f_2/\partial y_n \\ \vdots & & & \\ \partial f_m/\partial y_1 & \partial f_m/\partial y_2 & \dots & \partial f_m/\partial y_n \end{pmatrix} \tag{9}$$

$$\vec{f}^* = \begin{pmatrix} f_1(\vec{a}^*, \vec{y}^*) \\ f_2(\vec{a}^*, \vec{y}^*) \\ \vdots \\ f_m(\vec{a}^*, \vec{y}^*) \end{pmatrix} \tag{10}$$

In practice the constraints often depend directly on the four-vector components ($\vec{P} = (\vec{p}, E)$). By using the chain rule for derivatives $\partial \vec{f}/\partial \vec{y} = \partial \vec{f}/\partial \vec{P} \cdot \partial \vec{P}/\partial \vec{y}$ the calculation can be simplified.

In this new notation the likelihood which should be minimized becomes:

$$L = \Delta\vec{y}^T \mathcal{V}^{-1} \Delta\vec{y} + 2\lambda^T (\mathcal{A}\Delta\vec{a} + \mathcal{B}\Delta\vec{y} - \vec{c}) \ . \tag{11}$$

After differentiating with respect to $\vec{y}, \vec{a}$ and $\vec{\lambda}$ one gets the conditions for an extremum:

$$\begin{aligned} \mathcal{V}^{-1}\Delta\vec{y} + \mathcal{B}^T\vec{\lambda} &= 0 \\ \mathcal{A}^T\vec{\lambda} &= 0 \\ \mathcal{B}\Delta\vec{y} + \mathcal{A}\Delta\vec{a} &= c \ . \end{aligned} \tag{12}$$

These $(n+p+m)$ equations will be solved after each iteration for the unknown values $\Delta\vec{y}, \Delta\vec{a}$ and $\vec{\lambda}$. They can be written in only one equation with partitioned matrices:

$$\begin{pmatrix} \mathcal{V}^{-1} & 0 & \mathcal{B}^T \\ 0 & 0 & \mathcal{A}^T \\ \mathcal{B} & \mathcal{A} & 0 \end{pmatrix} \begin{pmatrix} \Delta\vec{y} \\ \Delta\vec{a} \\ \lambda \end{pmatrix} = \begin{pmatrix} 0 \\ 0 \\ c \end{pmatrix} \tag{13}$$

The inverse of the matrix given in eq. 13 can as well be written in a partitioned way:

$$\begin{pmatrix} \mathcal{V}^{-1} & 0 & \mathcal{B}^T \\ 0 & 0 & \mathcal{A}^T \\ \mathcal{B} & \mathcal{A} & 0 \end{pmatrix}^{-1} = \begin{pmatrix} C_{11} & C_{21}^T & C_{31}^T \\ C_{21} & C_{22}^T & C_{32}^T \\ C_{31} & C_{32} & C_{33} \end{pmatrix} \tag{14}$$

With the abbreviations given in eq. 15 the matrices C_{ij} can be defined as shown in eq. 16- 22.

$$\mathcal{V}_\mathcal{B} = \left(\mathcal{B}\mathcal{V}\mathcal{B}^T\right)^{-1} \qquad \mathcal{V}_\mathcal{A} = \left(\mathcal{A}^T\mathcal{V}_\mathcal{B}\mathcal{A}\right) \tag{15}$$

$$\begin{aligned} C_{11} &= \mathcal{V} - \mathcal{V}\mathcal{B}^T\mathcal{V}_\mathcal{B}\mathcal{B}\mathcal{V} && (16) \\ &\quad + \mathcal{V}\mathcal{B}^T\mathcal{V}_\mathcal{B}\mathcal{A}{\mathcal{V}_\mathcal{A}}^{-1}\mathcal{A}^T\mathcal{V}_\mathcal{B}\mathcal{B}\mathcal{V} && (17) \\ C_{21} &= -{\mathcal{V}_\mathcal{A}}^{-1}\mathcal{A}^T\mathcal{V}_\mathcal{B}\mathcal{B}\mathcal{V} && (18) \\ C_{22} &= {\mathcal{V}_\mathcal{A}}^{-1} && (19) \\ C_{31} &= \mathcal{V}_\mathcal{B}\mathcal{B}\mathcal{V} - \mathcal{V}_\mathcal{B}\mathcal{A}{\mathcal{V}_\mathcal{A}}^{-1}\mathcal{A}^T\mathcal{V}_\mathcal{B}\mathcal{B}\mathcal{V} && (20) \\ C_{32} &= \mathcal{V}_\mathcal{B}\mathcal{A}{\mathcal{V}_\mathcal{A}}^{-1} && (21) \\ C_{33} &= -\mathcal{V}_\mathcal{B} + \mathcal{V}_\mathcal{B}\mathcal{A}{\mathcal{V}_\mathcal{A}}^{-1}\mathcal{A}^T\mathcal{V}_\mathcal{B} && (22) \end{aligned}$$

With this notation the corrections to the parameters can be calculated by multiplication:

$$\Delta\vec{y} = C_{31}^T\vec{c} = \left(\mathcal{V}\mathcal{B}^T\mathcal{V}_{\mathcal{B}} - \mathcal{V}\mathcal{B}^T\mathcal{V}_{\mathcal{B}}\mathcal{A}\mathcal{V}_{\mathcal{A}}{}^{-1}\mathcal{A}^T\mathcal{V}_{\mathcal{B}}\right)\vec{c} \quad (23)$$

$$\Delta\vec{a} = C_{32}^T\vec{c} = \left(\mathcal{V}_{\mathcal{A}}{}^{-1}\mathcal{A}^T\mathcal{V}_{\mathcal{B}}\right)\vec{c} \quad (24)$$

$$\vec{\lambda} = C_{33}\vec{c} = \left(-\mathcal{V}_{\mathcal{B}} + \mathcal{V}_{\mathcal{B}}\mathcal{A}\mathcal{V}_{\mathcal{A}}{}^{-1}\mathcal{A}^T\mathcal{V}_{\mathcal{B}}\right)\vec{c} \quad (25)$$

The new parameters one gets as $\vec{y}' = \vec{y} + \Delta\vec{y} = \vec{y} + C_{31}^T\vec{c}$.

The variance of the fitted parameters $\vec{y}'$ can be calculated with error propagation from the covariance matrix of the measured parameters:

$$\mathcal{V}(\vec{y}') = (\mathcal{I} + C_{31}^T \underbrace{\frac{\partial\vec{c}}{\partial\vec{y}}}_{-\mathcal{B}})\mathcal{V}(\vec{y}) \quad (26)$$

$$= \underbrace{\mathcal{V} - \mathcal{V}\mathcal{B}^T\mathcal{V}_{\mathcal{B}}\mathcal{B}\mathcal{V} + \mathcal{V}\mathcal{B}^T\mathcal{V}_{\mathcal{B}}\mathcal{A}\mathcal{V}_{\mathcal{A}}{}^{-1}\mathcal{A}^T\mathcal{V}_{\mathcal{B}}\mathcal{B}\mathcal{V}}_{C_{11}} \quad (27)$$

The combined covariance matrix for the fitted parameters arises as:

$$\mathcal{V}\left[\begin{pmatrix}\vec{y}'\\ \vec{a}'\\ \vec{\lambda}'\end{pmatrix}\right] = \begin{pmatrix} C_{11} & C_{21}^T & 0\\ C_{21} & C_{22} & 0\\ 0 & 0 & -C_{33}\end{pmatrix} \quad (28)$$

The linearization is repeated until the defined convergence criteria are fulfilled. These should guarantee first that the χ^2-expression S only changes by a given value ε_S from one iteration to the next and second that the constraints are fulfilled to better than a given value ε_F:

$$\frac{S(n-1) - S(n)}{ndf} < \varepsilon_S \qquad \text{and} \qquad F_{(n)} = \sum_{k=1}^{m}\left|f_k^{(n)}(\vec{y},\vec{a})\right| < \varepsilon_F \quad (29)$$

In eq. 29 n denotes the number of the iteration and ndf is just the difference between the constraints and the amount of unmeasured quantities:

$$ndf = m - p \ . \quad (30)$$

To protect the fit from overshooting and jumping from a minimum, in every iteration n the value of the constraints $F_{(n)}$ is compared with the same value from the previous step $F_{(n-1)}$. If $F_{(n)} > F_{(n-1)}$, the corrections to the previous step are divided by two and different values are calculated. If this new correction cannot decrease the constraints with respect to $F_{(n-1)}$, the corrections are reduced further until $F_{(n)}$ becomes smaller than $F_{(n-1)}$. A fixed limit is set on the total amount of times this procedure is applied in every fit.

The analytical nature of this procedure ensures high speed performance, as well as reliable convergences and, therefore, is probably the most common mathematical framework utilized for constraint kinematic reconstructions in particle physics. The following sections illustrate the full potential of this kinematic fit approach.

3 Event Simulation

The events used throughout this paper are simulated with general tools available within the CMS Collaboration [7]. Events have been generated with either PYTHIA [8], ISAJET [9] or CompHEP [10], while the parton showering and fragmentation was performed by PYTHIA version 6.2. A full GEANT-4 detector simulation was used to simulate the CMS detector response. Low luminosity pile-up or minimum bias events (with a Poissonian mean of 3.5 pile-up collisions per bunch crossing reflecting the machine conditions at a luminosity of $2 \cdot 10^{33}$ cm^{-2}s^{-1}) were added to the signal events applying the same detector response simulation. The simulated events were reconstructed with the general software of CMS. General Data Summary Tapes or DST's were produced to facilitate the analyses. In the studies presented no background processes have been considered, as we aim to demonstrate relative improvements.

4 Kinematic Reconstruction of $Z \to \mu^+\mu^-$ Events

With roughly 20.000 recorded $Z \to \mu\mu$ decays per day with low luminosity settings, this decay channel is one of the important Standard Model calibration processes at the LHC. Due to its clear signature a selection and accurate reconstruction of the di-muon final state is straightforward. The excellent tracking capabilities in CMS allow a precise determination of the 3-momentum vector of each muon. Figure 2 shows an example of the di-muon invariant mass which represents an estimator of the underlying mass of the Z boson.

4.1 Mass constraints used for the alignment of tracker components

The resolution of the reconstructed 3-momentum vector of the muons can be further improved by imposing the external knowledge of the Z boson mass as measured by LEP via the kinematic fitting procedure described. Using

$$M(\mu_1, \mu_2) = M_Z \tag{31}$$

as external constraint results in a so-called *1C kinematic fit* [1)]. The use of the kinematic fit results in a strong correlation of the a priori uncorrelated momentum measurements of the two muons.

Figure 1 illustrates the difference between the *single track* and *double track* correlation of sensitive elements in the CMS tracker geometry [12]. In the two histograms shown in Figure 1 entries are made for all combinations of pairs of hits belonging to a 'track system', according to their relevant detector type and layer. The histrograms are normalized to the number of track systems. In the top histogram, the track systems are single tracks, whereas in the bottom histrogram, they are the pairs of double tracks corresponding to the muons from $Z \to \mu^+\mu^-$ decays. While the *single track* correlation only connects projective regions with each other, the use of the correlated two track system as obtained from the kinematic fit, results in correlations between detector components that are usually not connected via single tracks [2)]. Thus, complementary information to single collision tracks is provided for the internal alignment of the different detector elements. It is planned, in the future, to systematically exploit the use of invariant mass constraints for the tracker alignment.

4.2 A χ^2-scan procedure illustrated

Another possible application for kinematic mass constraints in well-measured systems, is the so-called χ^2-scan for different mass hypotheses. This technique has already been utilized at LEP to search for resonances whose exact invariant mass is unknown. A typical example for such a process at the LHC is the search for the Higgs boson in $H \to ZZ^{(*)} \to l^+l^-l'^+l'^-$. In theory there are two external kinematic mass constraints that can be utilized in the kinematic reconstruction:

- $M_H = M(l^+l^-l'^+l'^-)$
- $M_Z = M(l^+l^-)$

However, the invariant mass constraint of the Higgs is a prior unknown. Therefore, usually the search for a Higgs boson is carried out by searching for a mass peak above the continuum background. Unfortunately, this technique does not take into account the quality of the measured final state. All potential signal or background events typically enter with a weight of one in the mass histogram. In particular for the 4-muon final state this is not the optimal use of the available information content. Along with the measurements of the track parameters the CMS tracking has also been optimized to deliver a reliable estimate of the covariance matrix for each track. This covariance matrix represents an important element of the track measurements and should therefore also be included in an optimized analysis procedure. For $H \to ZZ^{(*)} \to l^+l^-l'^+l'^-$ this could be achieved by applying a *2C kinematic fit* that not only imposes the Z boson mass but also the Higgs mass constraint. Rather than looking for a mass peak in the invariant mass distribution, the search for the presence of the Higgs boson decay would be carried out by plotting the average χ^2 distribution for various sets of kinematic fits performed with different Higgs mass hypotheses. In

[1)] The fit package also foresees the use of a Gaussian smeared mass constraint $M(\mu_1, \mu_2) = \alpha M_Z$ where α represents a Gaussian distribution with a mean of one and a user defined width of σ_α.

[2)] Cosmic muons that traverse the entire detector and, thus, connecting the upper and lower barrel half with each other possess a similar property.

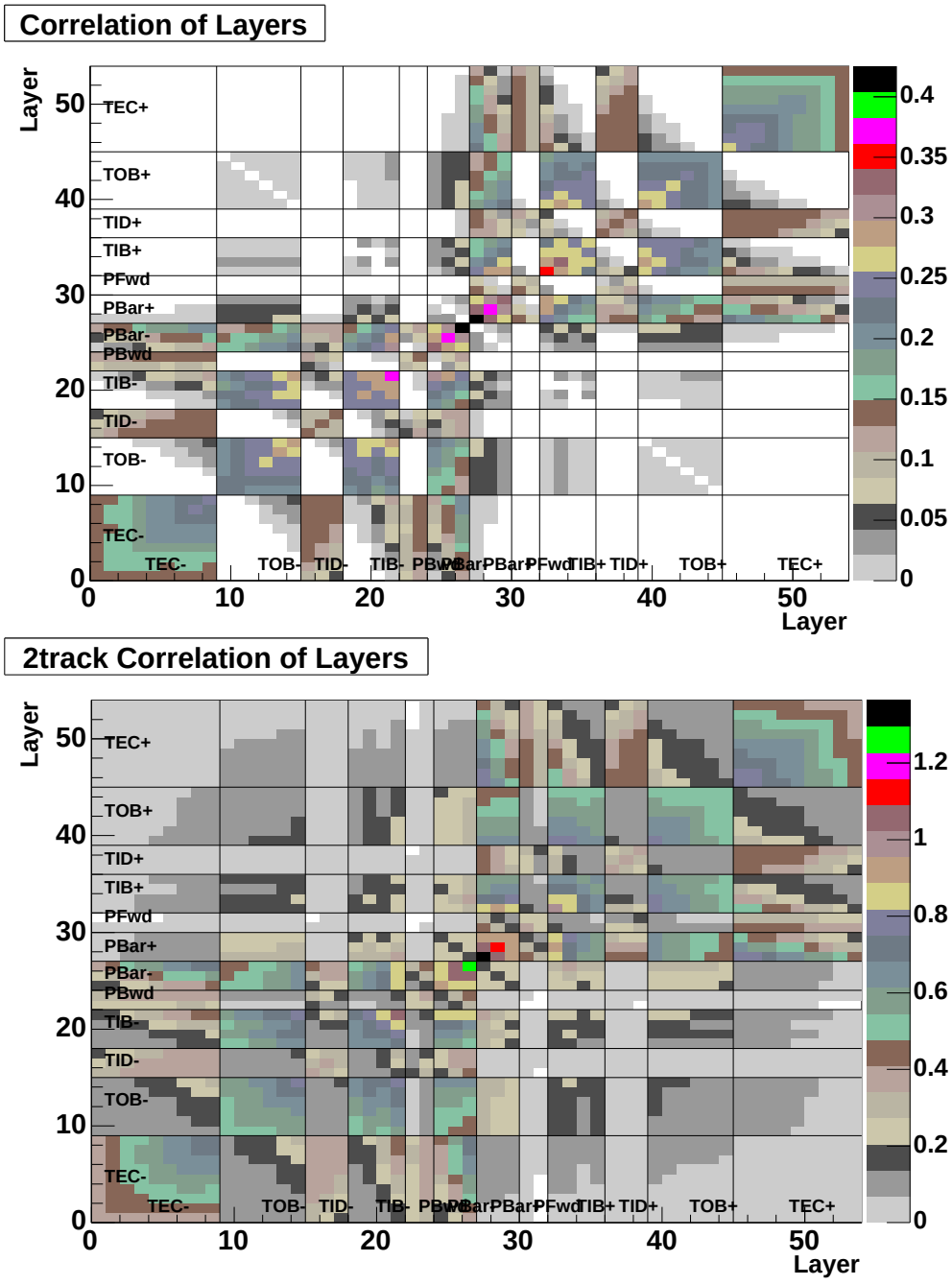

Figure 1: Single track and double track entries between tracking layers as described in the text.

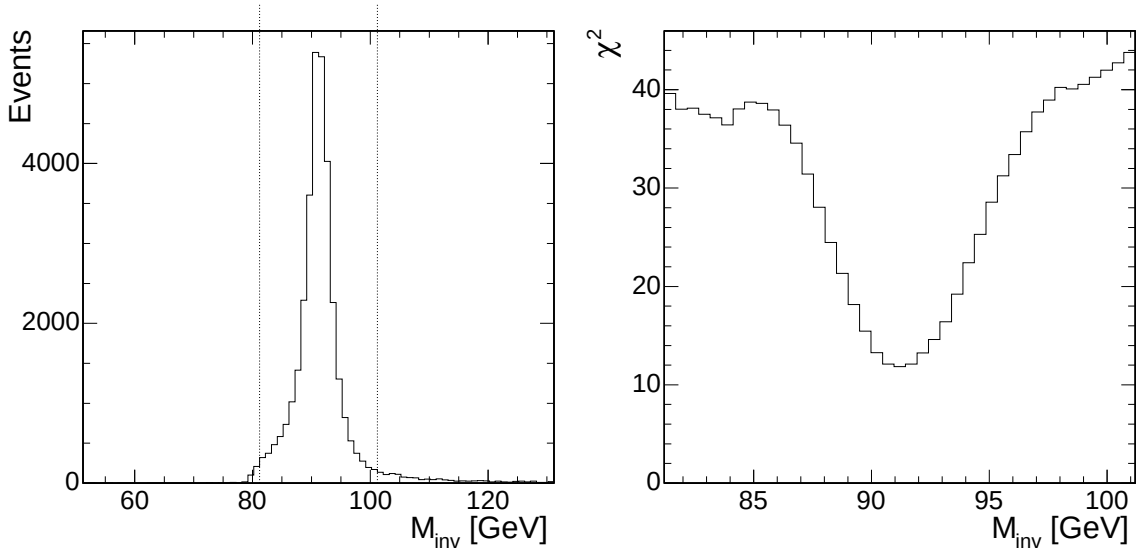

Figure 2: Mass (left) and χ^2 (right) distribution for different levels of tracker mis-alignment. The boarders of the χ^2 histogram are indicated in the mass distribution histogram with the two vertical dashed lines.

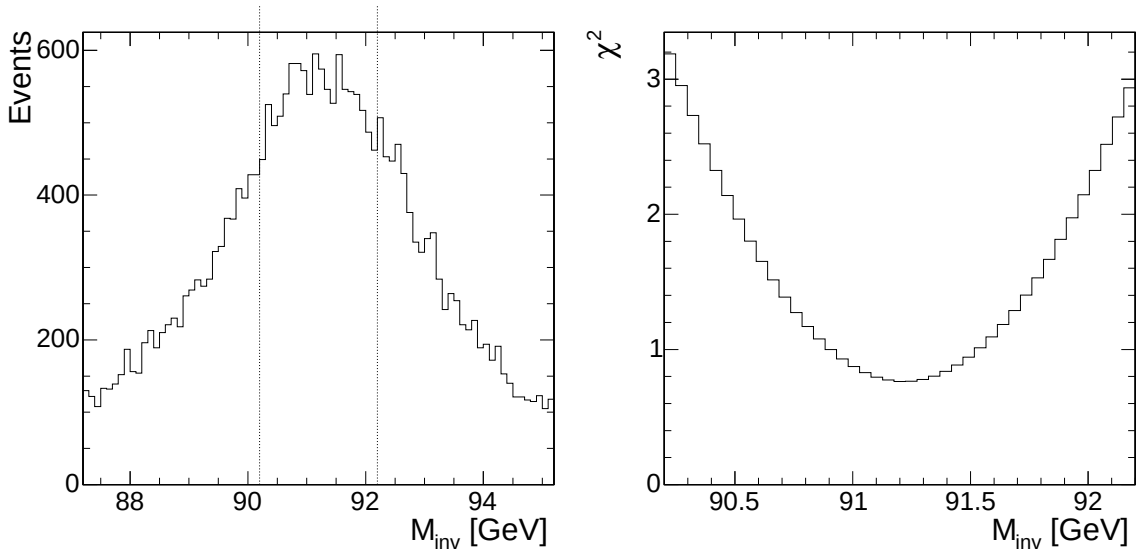

Figure 3: Mass (left) and χ^2 (right) distribution for different levels of tracker mis-alignment. The boarders of the χ^2 histogram are indicated in the mass distribution histogram with the two vertical dashed lines.

practice, a given set of selected events would be fitted N times each with a slightly different mass hypothesis. In the following this procedure is illustrated by using $Z \to \mu\mu$ events.

Figure 2 shows the mean χ^2 average for a given set of $Z \to \mu\mu$ events as function of the Z boson mass hypothesis in the kinematic fit. In order to cover a large phase space first a scan with a coarse binning in steps of 500 MeV/c^2 between 81 GeV/c^2 and 101 GeV/c^2 is used to identify a clear minimum in the χ^2. Once a minimum is identified, a much finer scan is performed around the discovered minimum. Figure 3 shows the result of this fine scan and for comparison also the corresponding invariant mass distribution is shown as obtained from the two reconstructed muons. The minimum of the average χ^2 is clearly compatible with the mass of the Z boson, 91.2 GeV/c^2, used to generate these simulated events. It is also important to note that the χ^2 minimum is around one which is fully consistent with the 1 degree of freedom used in the kinematic fit (i.e. the mass constraint). The $\Delta\chi^2 = 1$ contour results in 91.2 ± 0.7 GeV/c^2.

It is important to stress that this example is only meant as an illustration of an alternative analysis procedure devoted to the search for resonant structures with an unknown invariant mass. While it is possible to quantify for

the simple $Z \to \mu\mu$ case the potential sensitivity improvement of the χ^2-scan with respect to the sole use of the invariant mass distribution, we refrain from this pure academic exercise. We would like to point out that the use of the χ^2-scan procedure for well measured final states, like $H \to ZZ^{(*)} \to l^+l^-l'^+l'^-$, has the potential not only to cross check but also to improve the conventional analysis techniques based on the simple use of the reconstructed invariant mass as the sole search estimator.

5 Reconstruction of Semi-leptonic $\mathrm{t\bar{t}}$ Events

A wide field of interest at current and future hadron colliders is the domain of top quark physics. Measurements of the quantum numbers of this fermion and the properties of processes in which they appear are crucial both for the study of the Standard Model and in the search for new physics. The most essential challenge is the precise measurement of the mass of the top quark. It is another example of an analysis where kinematic fits are most useful. The kinematic fit probability of the hypothesed $t\bar{t}$ topology can be exploited as a variable to differentiate the true $t\bar{t}$ events from other final state processes, such as the different possible jet combinations in a given event.

5.1 Improvement in the Reconstructed Top Mass

The top quark has a branching ratio close to 100% to decay into a W boson and a bottom quark. When the W boson decays hadronically into two quarks which fragment and hadronize into jets of particles, the invariant mass of both the two-jet system from the W boson and the three-jet system from the top quark decay can be determined. By the use of a kinematic fit which forces the mass of the two-jet system from the W boson to match the precise measured W boson mass from Tevatron and LEP experiments, the resolution on the top quark mass can be improved.

In the case study presented we aim to show the relative improvement on the resolution on the top quark mass by applying a kinematic fit on the reconstructed top quark system which forces the W boson mass of $M_W = 80.426 \pm 0.034$ GeV/c^2 [13] to two of the three jets. Semi-leptonic $pp \to t\bar{t} \to bW\bar{b}W \to bq\bar{q}\bar{b}l\nu_l$ events are generated where exactly one of the two W bosons decays leptonically. The lepton was required to be a muon for simplicity. In total 200k events were simulated, which corresponds to an integrated luminosity of 1.68 fb^{-1} if $\sigma_{tt}^{NLO} = 800pb$. In these events we expect four hard jets, one hard lepton and missing transverse energy.

The event selection applied consist in sequential cuts on the reconstructed objects in the final state of the event. The jets in the events are reconstructed using the iterative cone algorithm with an opening angle of the cones of 0.5 rad. The clustering algorithm ran on calorimeter towers or so-called `EcalPlusHcalTower` objects in CMS above an energy threshold of 1 GeV. In the search for stable cones seeds are taken from those `EcalPlusHcalTowers` which exceed 1 GeV/c in transverse momentum. Calibration corrections are determined on the energy scale of the reconstructed jets as a function of the transverse momentum of the jet, and this in two adjacent ranges of pseudo-rapidity $|\eta| < 1.4$ and $|\eta| > 1.4$. In order to determine these corrections, only isolated jets are taken which match very well in angle with the generated primary parton direction. No differentiation was made between light and heavy flavoured quarks. The corrections make sure that on average the reconstructed energy of the jet matches the generated energy of the primary parton. To reconstruct the kinematics of the semi-leptonic $t\bar{t}$ event, the four jets with the highest E_T are selected as being the jets from the high-Q^2 process. For each of these four jets a b-tag probability was determined from its value for the b-tag discriminant [14]. Using the probability density functions $PDF_i(x)$ of the b-tag discriminant variable x for each quark flavour i, the b-tag probability was determined as:

$$L_b(x) = \frac{PDF_b(x)}{\sum_{i=1}^{5} PDF_i(x)} \quad . \tag{32}$$

The lepton was reconstructed and identified as described in [15]. Jets and leptons are only considered if they are in the reach of the CMS Tracker, being $|\eta| < 2.4$. The event selection criterion requires the event to have at least four jets which have a calibrated E_T above 30 GeV with exactly two with a b-tag probability larger than 60% and the selected lepton to have a transverse momentum p_T exceeding 20 GeV/c. To avoid jet energy scale calibration problems, only events are taken for which none of the four reconstructed jets overlap in an (η, ϕ)-metric.

Among the four reconstructed jets, three have to be choosen to form the hadronic decaying top quark. The efficiency or purity of this selection was largely enhanced by applying a likelihood ratio method combining the information from several sensitive variables [16]: a combined b-tag and anti-b-tag probability of the event, an angle between the jet from the leptonic decaying top quark and the lepton, a combined jet charge variable, etc. The theoretical correct jet pairing was defined as the one which results in the smallest angular differences between the four reconstructed jets and generated partons.

On the remaining events after the event selection the kinematic fit was applied. The input for this kinematic fit are the four jets and the lepton four-momentum together with the transverse missing energy as an estimate of the transverse component of the neutrino. For the jets a four-vector parametrization was used describing the deviation from the measured momentum in a local coordinate system:

$$\vec{u}_1 = \frac{\vec{p}_m}{|\vec{p}_m|}, \quad \vec{u}_2 = \frac{\vec{u}_3 \times \vec{u}_1}{|\vec{u}_3 \times \vec{u}_1|}, \quad \vec{u}_3 = \frac{\vec{u}_z \times \vec{u}_1}{|\vec{u}_z \times \vec{u}_1|} \ . \tag{33}$$

where u_z is the unit vector along the z-direction. The fitted momentum is parametrized with three parameters a, b, and c,

$$\vec{p}_f = a|\vec{p}_m|\vec{u}_1 + b\vec{u}_2 + c\vec{u}_3 \tag{34}$$

and the particle has a free floating fitted energy:

$$E_f = d \cdot E_{\mathrm{m}} \ . \tag{35}$$

In the parametrization for the lepton and the neutrino a special definition of the fitted energy is implemented. It's implementation is characterized by a constant ratio $E/|\vec{p}|$ equal to the measured ratio,

$$E_f = |\vec{p}_f| \frac{E_m}{|\vec{p}_m|}. \tag{36}$$

The neutrino longitudinal momentum was not reconstructed but determined from the fit. The covariance matrices which represent the resolution of these variables, are taken to be diagonal. The resolutions are differentiated as a function of the transverse momentum of the objects, being jets or lepton. Hence, each individual object obtains a covariance matrix according to its transverse momentum. For the transverse component of the neutrino, one fixed resolution was used. Two constraints are applied: one on the reconstructed hadronic W boson mass and one on the leptonic W boson mass. Both masses were forced to be equal to the current world average [13].

Within an event only jet combinations are considered which match the following criteria: the probability of the kinematic fit calculated from its χ^2/ndf should exceed 0.2, the difference between the fitted and reconstructed W

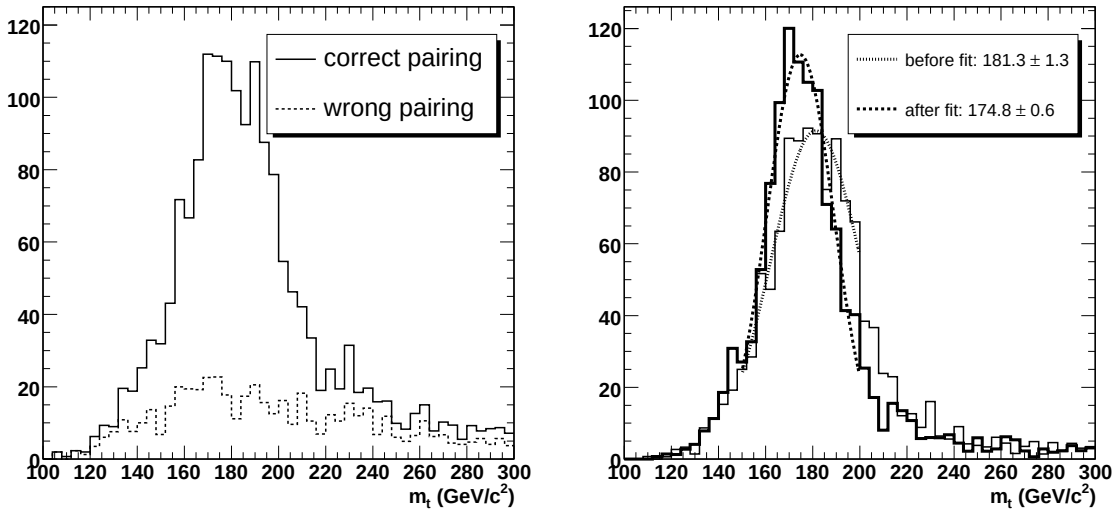

Figure 4: Distribution of the reconstructed top quark mass including wrong combinatorial jet pairings (left). Comparison of the reconstructed and fitted top quark mass distribution using only correct jet combinations (right).

boson mass should be less than 35 GeV/c^2, the fitted hadronic top quark mass should be less than 350 GeV/c^2 and the fitted leptonic top quark mass must be larger than 125 GeV/c^2.

The jet combination with the largest combined likelihood and fulfilling the above criteria was taken as the best pairing. From the combined likelihood variable, for the jet combinations, a probability was extracted for obtaining the theoretically correct combination. The event was only considered if the best pairing has a probability larger than 60% . In a large window around the expected top quark mass of about 175 GeV/c^2, the purity of the correct combinations was above 70%.

The distribution of the reconstructed top quark invariant mass using the selected events with their chosen pairing is shown in Figure 4. The contribution of the wrong jet combinations is illustrated. In the same figure, the distribution for only the correctly combined events is fitted with a Gaussian function and compared to the distribution obtained with the fitted top quark mass for the same events. The result of the Gaussian fit is

$$m_{t,rec} \;=\; 181.3 \;\pm\; 1.3\,\mathrm{GeV/c^2} \tag{37}$$

for the reconstructed top quark mass spectrum, and

$$m_{t,fit} \;=\; 174.8 \;\pm\; 0.6\,\mathrm{GeV/c^2} \tag{38}$$

for the fitted top quark mass spectrum. In order to obtain the same precision on the top quark mass without applying a kinematic fit, one would need 5 times more data compared to when a kinematic fit is applied. Also, the bias on the

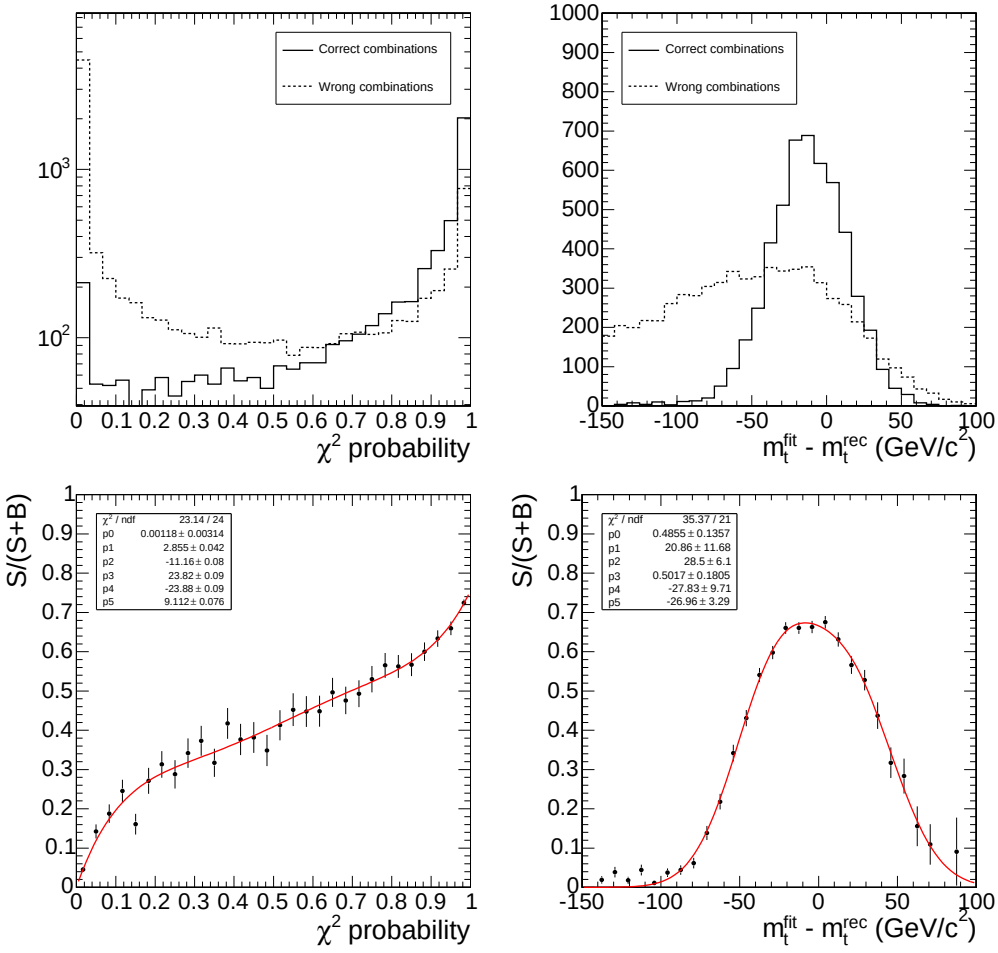

Figure 5: Distribution of the χ^2 probability of the kinematic fit (left) and the mass difference Δm_t (right) as defined in the text for correct and wrong jet associations. The bottom plots reflect the likelihood ratio S/(S+B) for obtaining the correct combination.

estimated top quark mass or its deviation from the input value M_t=175 GeV/c^2 in the simulation, is considerably reduced due to the application of a kinematic fit.

5.2 Classifying Jet Combinations with the Fit Probability

Inversely to the top quark mass measurement, the measured top quark mass from the Tevatron itself can be used as an additional input in the fitted event hypothesis. The reconstructed semileptonic $t\bar{t}$ event can be tested to match the kinematics of the true $t\bar{t}$ event. By forcing the reconstructed objects in the kinematic fit to fulfil both the precisely measured top quark mass and W boson mass constraints, the fit probability becomes a variable which can differentiate between the correct and wrong jet pairings.

After the event reconstruction, similar to the reconstruction for the top quark mass measurement, the kinematic fit is applied. The χ^2 probability resulting from the fit and the difference in reconstructed and fitted hadronic top quark mass $\Delta m_t = m_t^{rec} - m_t^{fit}$ have a strong discrimination power to suppress the combinatorial background. In Figure 5 these two variables are shown both for correct and wrong jet associations.

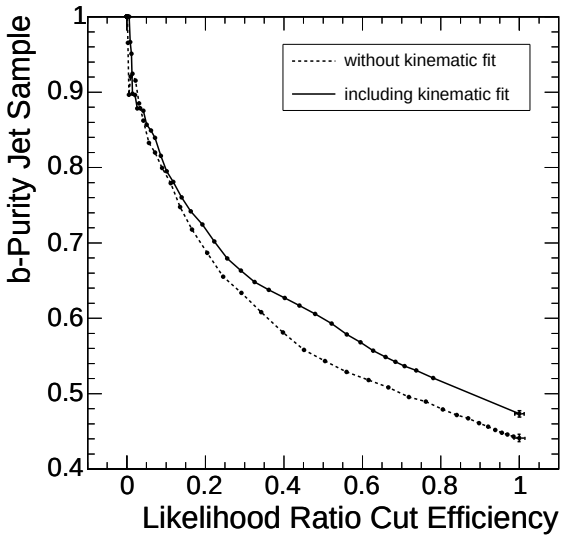

Figure 6: The b-purity of the selected jet sample as a function of the event selection efficiency with and without the use of a kinematic fit.

When applying a random jet combination procedure the efficiency of choosing the correct one is 1/12 or 8% . Because the jet topology in the final state is diluted due to radiation processes, the real efficiency will never reach 100% . Only in a fraction of the events a reconstructed jet combination matching the theoretical parton level is present. If one uses a likelihood ratio method combining the information of both observables χ^2 probability and Δm_t, the efficiency is increased to 51% when choosing the combination with the highest combined likelihood ratio value. This number has been obtained in events in which a theoretical correct jet combination is present, hence where 4 jets are reconstructed which match the primary partons to better than $\Delta R = 0.2$.

An analysis that benefits from fully constrained $t\bar{t}$ events is the measurement of *b*-tagging efficiencies on single leptonic $t\bar{t}$ events, from which a b-jet enriched jet sample is selected [16]. In these events two *b*-jets are present in the final state. The b-jet coming from the hadronically decaying top needs to be b-tagged to suppress the large $W+$ jets background. The b-enriched jet sample used for the measurement of the performance of b-tagging algorithms is selected from the b-jets present in the leptonically decaying top quark.

With the previously described observables, the χ^2 probability and Δm_t, together with some other kinematical variables, a combined likelihood ratio is constructed to distinguish correct from wrong jet associations. By cutting on this likelihood ratio value $\mathcal{L}$ the combinatorial background is suppressed and as a consequence also the b-jet purity of the jet sample obtained from the leptonically decaying top quark is increased.

In Figure 6 the b-jet purity of the jet sample is shown as a function of the event selection efficiency which is scanned by cutting on the combined likelihood ratio variable. The effect of including the two described variables from the kinematic fit is illustrated. A scan is made over several values of $\mathcal{L}$ and it is observed that over a large range an increase in the b-jet purity of about 5% is obtained by including the χ^2 probability and Δm_t variables.

6 Top Quark Reconstruction in Scalar Top Quark Decays

Extracting the top quark in a SUSY-type multi-jet event topology is challenging due to the large combinatorial background. The kinematic fit with constraints is a suitable and robust method to suppress such background.

The fit is used here to extract the top quark from the decay of a scalar top quark. In the signal sample considered, each event is required to contain a scalar top quark decaying as follows:

$$\tilde{t_1} \rightarrow tll\chi_1^0 \rightarrow Wbll\chi_1^0 \tag{39}$$

where χ_1^0 is the lightest supersymmetric particle, stable and weakly interacting, and the W decays inclusively.

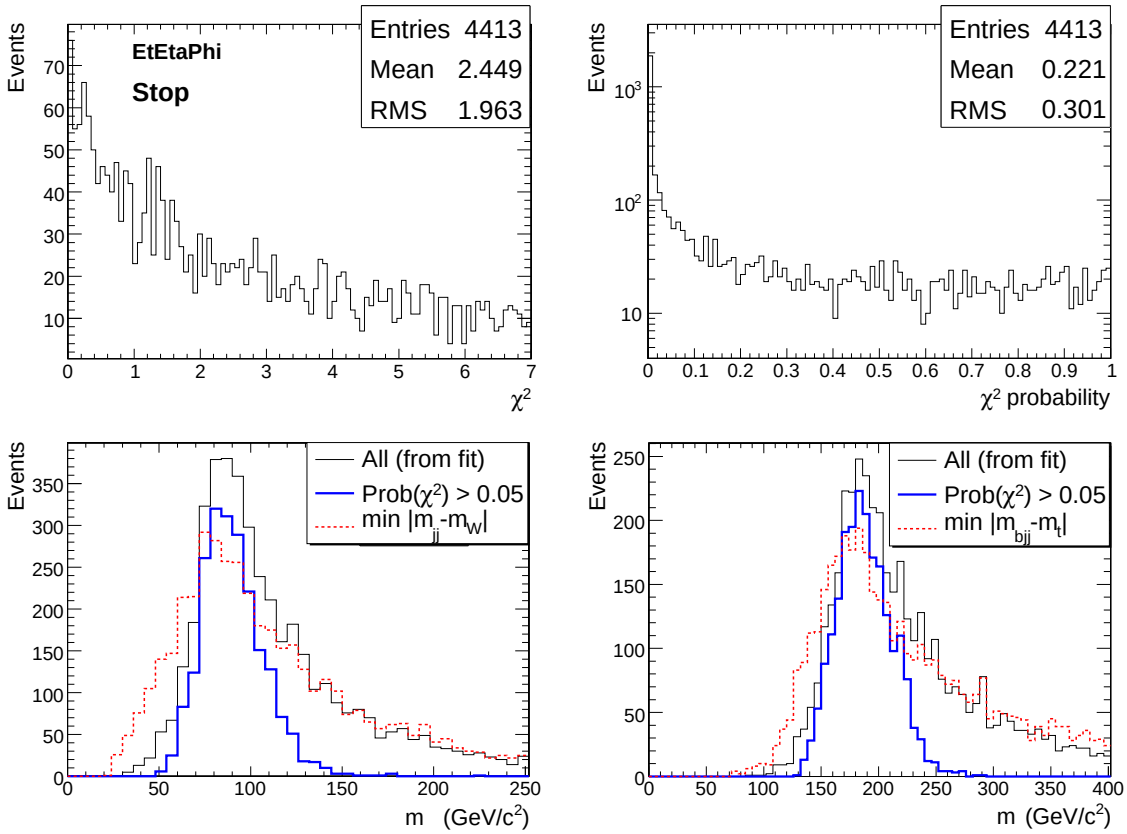

Figure 7: The distribution of minimum χ^2 (upper left) and χ^2 probability distribution (upper right). The di-jet (lower left) and tri-jet (lower right) invariant mass for the best combination (least χ^2). The thick (blue) lines show the corresponding distributions after applying the cut on the χ^2 probability. The dotted (red) lines show a general method to extract the top quark described in the text. The fit results in narrower distributions in the expected regions.

In total 6629 signal events were simulated and reconstructed for this study. The method used to reconstruct jets is the iterative cone algorithm with 0.5rad cone opening angle and applying the E_T recombination scheme. The noise threshold applied on the calorimeter towers used as input for the jet clustering algorithm are η dependent. In addition, those towers that contain energy from an isolated electron are rejected from the list of input towers used in the jet clustering. Calibrated jets with $E_T \geq 30$ GeV and $|\eta| \leq 2.5$ are considered. Jets are calibrated using corrections from photon-jet balancing studies [17]. The b-tagging is done using an impact parameter algorithm [18].

The top quark mass and W boson mass are the two constraints used in this kinematic fit example. Three jets, one of which is $b-$tagged are used as inputs to the fit. The momentum vector of the jets is parametrized as

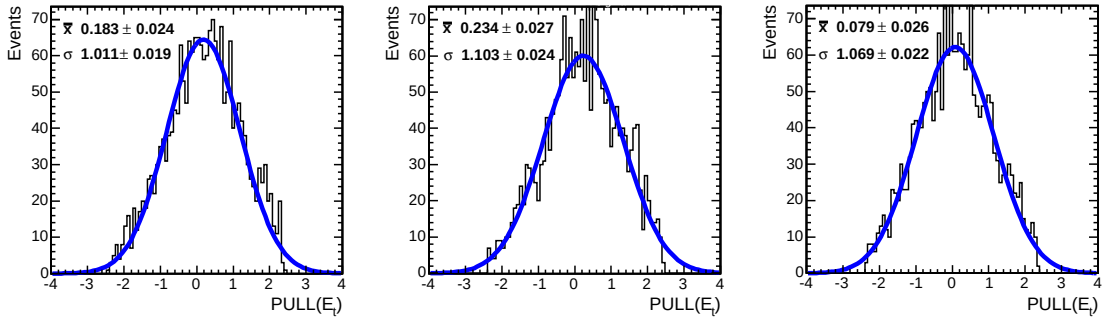

Figure 8: *PULL*-distributions of the E_T estimator of the three jets used in the fit when the χ^2 probability is greater than 0.05. The third jet (most right plot) was chosen among the *b*-tagged jets. The mean($\bar{x}$) and σ of the gaussian fit are shown for every distribution.

$$\vec{p}_f = \begin{pmatrix} E_T \cos\phi \\ E_T \sin\phi \\ E_T \sinh\eta \end{pmatrix} . \tag{40}$$

and the energy E can be derived easily from the transverse energy E_T,

$$E = E_T \cosh\eta \quad . \tag{41}$$

In this parameterization, jets are considered as massless objects. The covariance matrices are assumed to be diagonal, since the resolutions of the different parameters are considered uncorrelated. The E_T, η and ϕ jet resolution parameterizations used in the fit can be found in [19] as a function of the simulated true jet energy. In every event, the converging jet combination that minimizes the χ^2 is found. If the χ^2 probability is less than 0.05 ($\chi^2 > 6$), the event is rejected.

Figure 7 shows the di-jet ($W \to q\bar{q}$) and tri-jet ($t \to Wb \to q\bar{q}b$) invariant mass distributions before and after the cut on the χ^2-probability. The χ^2 distribution and its probability distribution are shown in the same figure.

Using the fit, 16% of the reconstructed top quarks are closer than $\Delta R = \sqrt{\Delta\eta^2 + \Delta\phi^2} = 0.5$ to a generated top quark that decays hadronically. After applying the cut on the χ^2 probability this number (refered to as purity) increases to 20%. A simple approach to extract the top quark but not using the kinematic fit is by finding the di-jet system with the closest invariant mass to m_W = 80 GeV/c^2 as the W candidate. The top quark candidate is then found by combining the di-jet system with a *b*- jet that forms the closest tri-jet invariant mass to m_t = 175 GeV/c^2. The corresponding distributions are shown in Figure 7 (bottom) with dotted (red) lines. Using this approach the purity is 11% , about half of that obtained with the kinematic fit approach.

The *PULL* [3)]-distributions of the transverse energies of three jets (Figure 8) are sufficiently close to a Gaussian with mean of zero and sigma of one as expected.

The reconstructed and fitted energy resolutions for both the top quark and the W boson, are shown in Figure 9. The fit improves the resolution of the measured energy of the W boson and the top quark by 33% and 62%, respectively.

7 Higgs Reconstruction in $t\bar{t}H$ Decays

The associated Higgs production together with a $t\bar{t}$ pair has been identified as crucial in the study of the CMS capability in discovering and measuring Higgs physics. The Higgs decay into $b\bar{b}$ is dominant for a Higgs boson with a mass below 130 GeV/c^2. While the direct Higgs production is impossible to detect, due to the huge QCD

[3)] The pull for every fitted parameter y_i is defined as the ratio of the shift in the parameter and the variance of the shift. Here that we compare the fitted values with the reconstructed ones, the pull can be written as $PULL(y_i) = \frac{y_{i,meas} - y_{i,fit}}{\sqrt{\sigma^2_{i,meas} - \sigma^2_{i,fit}}}$.

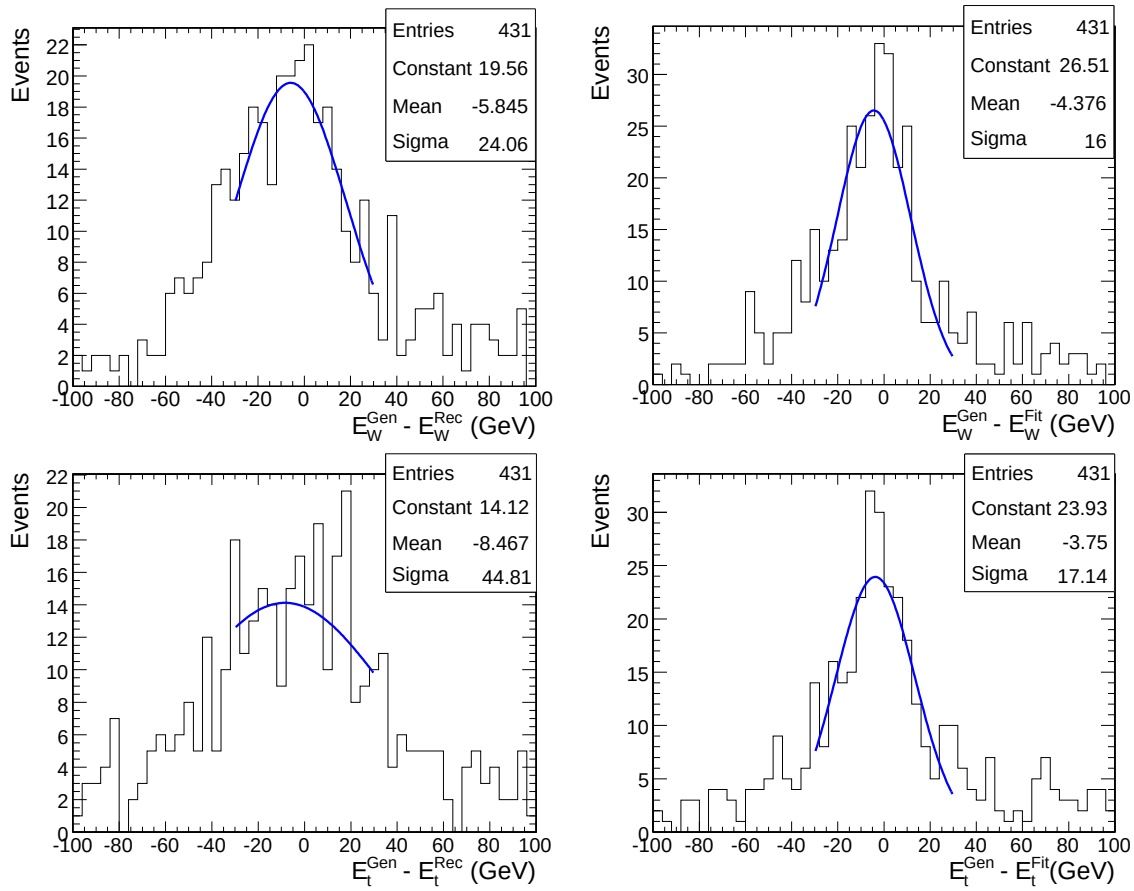

Figure 9: The top quark (lower) and W boson (upper), reconstructed (left) and fitted (right), energy resolution. All comparisons are done if the fit probability is greater than 0.05. The resolution is illustrated by fitting the central parts of the distributions (-30, 30) with a Gaussian function.

background, the Higgs production in association with a $t\bar{t}$ pair is promising to contribute to an early discovery and allows precision measurements, such as the top-Higgs and b-Higgs Yukawa couplings. The process considered is

$$pp \to t\bar{t}H \to WbW\bar{b}\bar{b} \ . \tag{42}$$

The final state topology has the following signature: 6 hadronic jets, an isolated muon and missing energy coming from the neutrino in one of the two W boson decays. Four of the hadronic jets in the final state originate from a b-quark. The very complicated signature of this channel leads to a high number of possible jet pairings to reconstruct the complete event and thus the mass of the Higgs boson. The kinematic fit described is a useful tool to resolve this combinatorial problem.

This analysis is based on 50k signal events generated with a nominal Higgs boson mass of 120 GeV/c^2. An event selection is applied in order to require reconstructible events. Jets are reconstructed with the iterative cone algorithm with an opening angle of 0.5 rad. The inputs for the jet reconstruction are `EcalPlusHcalTowers` above tower energy thresholds depending on their pseudo-rapidity value and tuned to minimize the effect of underlying events. Reconstructed jets are calibrated to match on average the energy of a generated jet determined from the kinematics of all generated particles radiated in a cone around the direction of the reconstructed jet. The b-tagging algorithm applied is the combined b-tag [14] providing a b-tag discriminant. A jet is defined as a b-jet when this b-tag discriminant is larger than 1.5.

At least 6 jets with a reconstructed E_T above 10 GeV and a calibrated E_T greater than 20 GeV are required. Only jets in the Tracker acceptance ($|\eta| < 2.4$) are considered and at least four out of six jets have to be b-tagged. The reconstructed muon from the W boson decay in the final state is identified using a likelihood approach

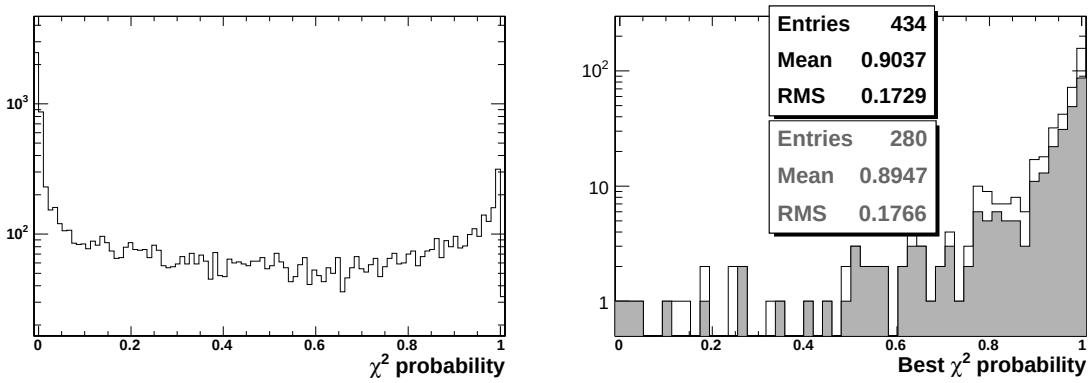

Figure 10: Distribution of the χ^2 probability for all combinations (left) in $t\bar{t}H$ events and the distribution of the largest χ^2 probability (right). The white histogram refers to events where the correct jet combination has the largest χ^2 probability, while the gray histogram refers to the events where the wrong combination has the largest χ^2 probability.

combining several kinematic observables: the transverse momentum of the muon candidate, the ΔR between the muon candidate and the closest jet, the muon impact parameter significance and the total transverse momentum of all tracks or calorimeter clusters in an isolation cone. The transverse missing energy of the event E_T^{miss} takes into account the energy correction from calibration and muons, it is computed as

$$\vec{E}_T^{miss} = \sum_{it} \vec{E}_T^{tower} - (\sum_{ijr} \vec{E}_T^{RawJet} - \sum_{ijc} \vec{E}_T^{CaliJet}) + \sum_{im} \vec{E}_T^{Muon} \tag{43}$$

where *it* runs over the `ECalPlusHCalTowers`, *ijr* over the reconstructed jets, *ijc* over the calibrated jets and *im* over the muons in the event. The E_T^{miss} is taken to be the transverse energy of the neutrino and the longitudinal component is computed from the W momentum conservation

$$m_W^2 = (E^\mu + E^\nu)^2 - (\vec{p}^\mu + \vec{p}^\nu)^2 \ . \tag{44}$$

The last equation gives real solutions for p_z^ν in 66% of cases, in the remaining 34% the neutrino is assumed to be collinear with the muon. Around 1% of the signal events pass the event selection. The kinematic fit is applied to statistically test true $t\bar{t}H$ event topologies in resolving the jet combinatorics of the remaining reconstructed events.

The value of the fit probability is used to identify the best jet combination to connect the two non-b jets to the W boson decay and two b jets to the top quark decays. Every jet combination of two non-b jets with an invariant mass within two standard deviations from the W boson mass is considered in the combinatorics for the hadronic W boson, and every combination of two b jets is considered to reconstruct the hadronic and leptonic top quarks. When there are two solutions for the longitudinal component of the neutrino momentum, both are used. Four mass constraints are forced in the kinematic fit, the leptonic and hadronic W boson masses and the leptonic and hadronic top quark masses. The two b-jets which provide the largest value of the kinematic fit probability are taken to reconstruct the two top quarks and the remaining b-jet pair is assigned to the Higgs boson.

The four-vector parametrization of the jets is in spherical coordinates with three parameters r, θ, and ϕ parametrizing the momentum vector,

$$\vec{p}_f = \begin{pmatrix} r\cos\phi\sin\theta \\ r\sin\phi\sin\theta \\ r\cos\theta \end{pmatrix} \ . \tag{45}$$

and a free floating energy,

$$E_f = d \cdot E_m \ , \tag{46}$$

parametrized with an additional parameter d. For the muon and the neutrino a cartesian four-vector parametrization is used. The fitted momentum vector is described by three parameters x, y, and z with

$$\vec{p}_f = x\vec{u}_x + y\vec{u}_y + z\vec{u}_z \tag{47}$$

and they have a fixed mass m, therefore the fitted energy is defined by

$$E_f = \sqrt{|\vec{p}_f|^2 + m^2} \ . \tag{48}$$

The covariance matrices are assumed to be diagonal. The jet resolutions are parametrized as a function of the reconstructed jet energy, while fixed resolutions are used for the muon and neutrino momenta.

The distribution of the largest fit probability value in the event is shown in Figure 10 for correct and wrong jet combinations. The correct jet pairing is defined as the one which results in the smallest angular differences between the six reconstructed jets and generated partons.

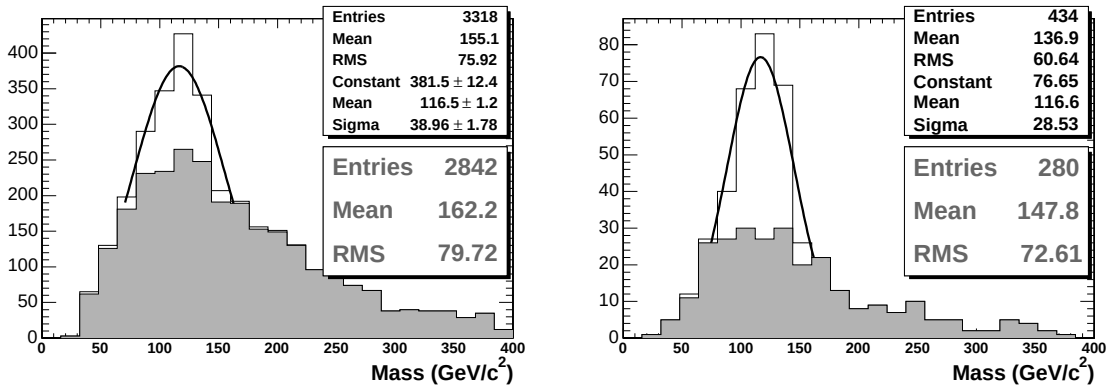

Figure 11: Distributions of the reconstructed Higgs boson mass from all jet combinations (left) and from those maximizing the kinematic fit probability (right). The gray histograms refer to wrong combinations and the white histograms to the correct combinations.

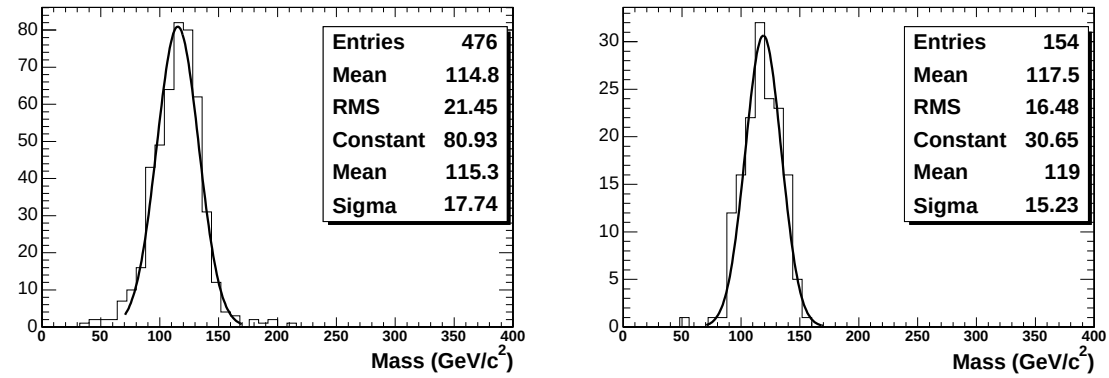

Figure 12: Distributions of the reconstructed Higgs boson mass from good combinations (left) and from good combinations found by maximizing the kinematic fit probability (right).

This method using the kinematic fit probability has been compared with the reconstructed Higgs boson mass spectrum with all accepted jet combinations of the four selected b-tagged jets. Figure 11 shows the reconstructed Higgs boson mass distribution from all jet combinations and from these which maximize the kinematic fit probability of the event. The contribution of the wrong combinations is also shown for both methods. The use of the kinematic fit significantly improves both the pairing efficiency, defined as the ratio of the correct over all combinations, and the resolution. The pairing efficiency increases from 14.3%, using all combinations method, up to 35.5%, using the kinematic fit. In addition the Gaussian fitted width of the peak of the distribution is reduced by 10 GeV/c^2 if

the kinematic fit is used to select the jet pairing. The distribution of the reconstructed Higgs boson mass with only the good combinations of the selected events is shown in Figure 12 together with the sub-set of good combinations found by the kinematic fit. The fitted Higgs boson mass distribution has a mean value of 119 GeV/c^2 very close to the nominal one of m_H=120 GeV/c^2 and it is narrower with respect to the reconstructed distribution, demonstrating that by applying the kinematic fit on the $t\bar{t}$ part of the event also results in a better reconstruction of the Higgs boson mass.

8 Summary

Fitting event topologies with kinematic constraints has become a standard technique in the analyses of high energy collisions. In this paper a non-linear least square method with Lagrange multipliers has been applied to force these kinematic constraints. The constraint fitting technique can on an event-by-event basis improve the resolution of invariant masses which have well known particles in their decay and the kinematic topology of the observed event can be statistically tested to match a hypothesed topology. It was demonstrated in different analyses that the use of the kinematic fit method significantly improves the results. For example in the reconstruction of the top quark mass ($t \to bW \to bq\bar{q}'$) or the Higgs boson mass ($H \to ZZ^{(*)} \to l^+l^-l'^+l'^-$), where respectively the W boson and the Z boson are present in the decay. The kinematic fits will not only improve the resolution on the reconstructed mass, but it was also shown that they create mass estimators which are less sensitive to systematic miscalibrations in the reconstruction of the kinematics of the decay objects. In many interesting event topologies at the LHC, a large number of hadronic jets are present in the final state. This feature increases the ambiguity for choosing the correct jet combination in the reconstruction of the decay tree in the event. Kinematic fits are shown to be useful in differentiating between correct and wrong jet combinations, and therefore also between signal and background events. The χ^2 probability of the fit becomes an event observable which can be used to differentiate between true and wrong hypotheses. Examples are presented in the selection of the correct jet combination in $t\bar{t}$ events, in the search for scalar top quarks and in the search for the Standard Model Higgs boson ($H \to b\bar{b}$) in association with top quarks. In all use cases a significant improvement is obtained when applying the fitting methods described.

Acknowledgement

Originally the fit package was called ABCFIT and has been developed by J.B.Hansen and O.Buchmüller for the ALEPH Collaboration. In 2002 the package was introduced in the software framework of BaBar and mainly used for the kinematic reconstruction of semileptonic B decays. In 2004 two BaBar PhD students, Verena Klose and Jan Eric Sunderman, from TU Dresden have translated the Fortran based code structure in C++. It was carefully tested that the original performance and numerically stability was not affected by the translation process. The C++ version of the package was kindly provided by them to be used within the CMS software framework.

References

[1] LEP Electroweak Working Group, *'A Combination of Preliminary Electroweak Measurements and Constraints on the Standard Model'*, CERN-PH-EP/2005-051 and hep-ex/0511027 (November 2005).

[2] The BaBar Collaboration, Aubert, B. *et al., 'Measurements of moments of the hadronic mass distribution in semileptonic B decays'*, Phys. Rev. **D**69, 2004, 111103, hep-ex/0403031.

[3] The BaBar Collaboration, Aubert, B. *et al., 'Determination of the branching fraction for $B \to X_c l\nu$ decays and of $|V_{cb}|$ from hadronic mass and lepton energy moments'*, Phys. Rev. Lett. 93, 2004, 011803, hep-ex/0404017.

[4] The BaBar Collaboration, Aubert, B. *et al., 'Measurement of the inclusive charmless semileptonic branching ratio of B mesons and determination of $|V_{ub}|$'*, Phys. Rev. Lett. 92, 2004, 071802, hep-ex/0307062.

[5] The LEP Collaborations, *'Search for the Standard Model Higgs Boson at LEP'*, Phys. Lett. **B** 565(2003)61-75.

[6] R.K. Bock et al., *'Formulae and methods in experimental data evaluation, with emphasis on high energy physics v.3 : Articles on statistical and numerical methods'*, CERN, Geneva (1983).

[7] The CMS Collaboration, *'CMS Object-Oriented Reconstruction page'*, `http://cmsdoc.cern.ch/orca/`.

[8] T.Sjöstrand, P.Edén, C.Friberg, L.Lönnblad, G.Miu, S.Mrenna and E.Norrbin, *'High-Energy-Physics Event Generation with PYTHIA 6.1'*, Computer Phys. Commun. 135 (2001) 238 (LU TP 00-30, hep-ph/0010017).

[9] H.Baer, F.E.Paige, S.D.Protopescu, and X.Tata, *'A Monte Carlo Event Generator for pp, $\bar{p}p$, and e^+e^- Interactions'*, hep-ph/0312045.

[10] A.Pukhov *et al.*, *'CompHEP - a package for evaluation of Feynman diagrams and integration over multi-particle phase space'*, Preprint INP MSU 98-41/542, hep-ph/9908288.

[11] S.Agostinelli *et al.*, *'GEANT4: A Simulation Toolkit'*, NIM **A** 506 (2003), 250-303.

[12] CMS Tracker Collaboration, *'The Tracker Project Technical Design Report'*, CERN/LHCC 98-6, and Addendum CERN/LHCC 2000-016.

[13] S.Eidelman *et al.*, *'Particle Data Group'*, Phys. Lett. **B** 592, 1 (2004).

[14] C. Weiser, *'A Combined Secondary Vertex Based B-Tagging Algorithm in CMS'*, CMS Note 2006/014.

[15] J.D'Hondt, J.Heyninck, S.Lowette, *'Lepton reconstruction in single-leptonic $t\bar{t}$ events'*, CMS Note 2006/024.

[16] S.Lowette, J.D'Hondt, J.Heyninck and P.Vanlaer, *'Offline Calibration of b-jet Identification Efficiency'*, CMS Note 2006/013.

[17] V.Konoplianikov, A.Ulyanov, O.Kodolova, *'Jet Calibration using γ + Jet events in the CMS Detector'*, CMS Note in preparation.

[18] CMS Collaboration, *'The Trigger and Data Acquisition project,Volume II'*, CERN/LHCC 2002-26,CMS TDR 6.2,15 December 2002.

[19] A.Heister *et al.*, *'Measurement of Jets with the CMS Detector at the LHC'*, CMS Note in preparation.